# Modulational instability of $F = 2$ spinor condensates

T. Mithun and K. Porsezian

*Department of Physics, School of Physical, Chemical and Applied Sciences, Pondicherry University, Pondicherry 605 014, India*

(Received 30 September 2011; published 10 January 2012)

We first analytically examine the occurrence of modulational instability in all phases of $F = 2$ spinor homogeneous condensate from the possible stationary solutions. Then we numerically show the similar results by extending our analysis to trapped condensates (inhomogeneous). From both analyses we conclude that modulation instability depends on the relative phase between the components and initial population for the polar phase. We also observe spin-mixing dynamics during evolution of the spinor condensate.

DOI: 10.1103/PhysRevA.85.013616 PACS number(s): 03.75.Mn, 05.30.Jp

## I. INTRODUCTION

The experimental realization of macroscopic accumulation of bosons in quantum mechanical ground state at low temperature, so-called Bose-Einstein condensate (BEC), in dilute atomic gases [1–3] evoked some novel phenomena in the fields of atom optics and condensed-matter physics. The nonlinearity arising from the interatomic interactions and the trapping potential play crucial roles in the behavior of a condensate whose time evolution is described by a Gross-Pitaevskii (GP) equation; meanwhile, the use of an optical trap for the confinement of BEC instead of magnetic trap leads to dynamical change in the direction of the spin due to the interparticle interaction. These BECs with internal spin degrees of freedom (spinor condensates) show complex quantum structures [4].

Spinor condensates exhibit rich quantum dynamics [5–10] due to the vector properties of the condensate order parameter and the nonlinear spin-spin interactions. After its basic theoretical framework [11,12] and experimental demonstration [13], its rich physics has already been reported. One of interesting properties is the modulational instability (MI) of spinor condensates [10,14–17], which gives some analogy between coherent matter waves and light waves in nonlinear optics. Since MI of the $F = 1$ spinor case has predicted some property of coherent matter wave it was clear that studying instability of $F = 2$ will give extra properties due to the extra interaction parameter appearing in the $F = 2$ case (arising from increase in the spin value). MI phenomena arising from the nonlinear interatomic interactions give a relevant mechanism to learn some dynamical processes in BEC systems [14,18,19].

Because of the extra parameter in $F = 2$ compared to the $F = 1$ case, there exist four phases, namely, ferromagnetic, uniaxial nematic (UN), biaxial nematic (BN), and cyclic [33]. UN and BN phases are often referred to as polar or antiferromagnetic phase. Condensate may be in one of these phases depending on the scattering lengths and the corresponding ground-state structure [20]. The dynamical properties of these phases are very different in nature. Since only the ferromagnetic phase is showing MI for the $F = 1$ case it was a quest to clarify whether all phases of $F = 2$ spinor condensate show modulation instability of one or two. From the reported results of the dynamical instability of the $F = 2$ spinor condensate [16,21], it is clear that detailed analysis will give some more interesting new properties. Also, a detailed study of the dynamics of components in all phases during MI is required.

In this paper, we show the modulation instability in the $F = 2$ case arising from the coupling between spin degrees of freedom by following the same analytical method used for the $F = 1$ case by Robins *et al.* [14]. It shows that ferromagnetic and cyclic phases show the modulation instability but the initial population and phase of the components decide the modulation instability of the polar case. This result is almost same as in Refs. [10,22]; that is, for two-dimensional BEC (TEBC) the sign of the interaction alone cannot determine the stability of system and the evolution of the spinor condensate is sensitive to its initial phase and population distributions, respectively. The peculiarity of polar state, its dependence on relative phases, shows that MI in this state is similar to the chemical potential in cyclic state as in Ref. [16]. It also gives some details about spin-mixing dynamics in the $F = 2$ case during the evolution from initially polarized stable stationary state.

The paper is organized as follows. In Sec. II, a model for the $F = 2$ spinor BEC is introduced. The MI analysis is performed in Sec. II A. In Sec. III, we present the results obtained from numerical simulation of the coupled dimensionless multicomponent GP equations. We conclude with all our observations and results in Sec. IV.

## II. MODEL

For the $F = 2$ spinor condensate there are five spin degrees of freedom represented by magnetic quantum number, $m = -2,-1,0,1,2$ due to the vectorial nature. As a result the order parameter (wave function of the condensate) characterizing the $F = 2$ spinor condensate having five components are $\Phi = (\phi_2,\phi_1,\phi_0,\phi_{-1},\phi_{-2})$. The multicomponent GP equations describing the evolution of the wave function of the condensate can be obtained from the derivative of the energy functional, $i\hbar\frac{\partial\Phi}{\partial t} = \frac{\delta E[\Phi]}{\delta\Phi^*}$. Here the energy functional, $E[\Phi]$ is of the form [23]

$$E[\Phi] = \int d\mathbf{r}\left\{\Phi^*\left[-\frac{\hbar^2}{2m}\nabla^2 + V_T(\mathbf{r})\right]\Phi + \frac{c_0}{2}n^2 + \frac{c_2}{2}\mathbf{f}^2 + \frac{c_4}{2}|\Theta|^2\right\}. \quad (1)$$

This is the Hamiltonian for the spinor BEC in the optical trap in the magnetic field free case. The coupling constants $c_i$'s ($i = 0,2,4$) are real and govern the nonlinear interaction

 

between different spin components of the condensate. Here $c_0 = \frac{4g_2+3g_4}{7}$, $c_2 = \frac{g_4-g_2}{7}$, and $c_4 = \frac{7g_0-10g_2+3g_4}{7}$. Here the suffixes 0, 2, and 4 denote the total spin (for $F = 2$, total spin 0, 2, or 4 are possible for bosons) and $g_i = \frac{4\pi\hbar^2}{m}a_i$ $(i = 0,2,4)$, where $a_i$'s are scattering lengths of two colliding bosons. $V_T(\mathbf{r})$ is the trapping potential. The number density,

$$n = \sum_{\alpha=-2}^{2} \phi_\alpha^* \phi_\alpha, \tag{2a}$$

and the spin densities $\mathbf{f} = (f^x, f^y, f^z)$. Here $\mathbf{f}^i$ are spin matrices for $F = 2$,

$$f^i = \sum_{\alpha,\beta=-2}^{2} \phi_\alpha^* \mathbf{f}^i_{\alpha\beta} \phi_\beta. \tag{2b}$$

The spin singlet-pair amplitude is given by

$$\Theta = \frac{1}{\sqrt{5}}(2\phi_2\phi_{-2} - 2\phi_1\phi_{-1} + \phi_0^2); \tag{2c}$$

here $\Theta = \sum_{j,j'} \langle 00|2j;2j'\rangle \phi_j \phi_{j'}$ annihilates a pair of bosons at a position and $\langle 00|2j;2j'\rangle$ is Clebsch-Gordan coefficient.

From Eq. (1) the coupled field equations are obtained in the form

$$i\hbar\frac{\partial\phi_{\pm2}}{\partial t} = L\phi_{\pm2} + c_2(\pm2f^z\phi_{\pm2} + f^{\mp}\phi_{\pm1}) + \frac{c_4}{\sqrt{5}}\Theta\phi_{\mp2}^*, \tag{3a}$$

$$i\hbar\frac{\partial\phi_0}{\partial t} = L\phi_0 + c_2\frac{\sqrt{6}}{2}(f^+\phi_1 + f^-\phi_{-1}) + \frac{c_4}{\sqrt{5}}\Theta\phi_0^*, \tag{3b}$$

$$i\hbar\frac{\partial\phi_{\pm1}}{\partial t} = L\phi_{\pm1} + c_2\left(f^{\pm}\phi_{\pm2} \pm f^z\phi_{\pm1} + \frac{\sqrt{6}}{2}f^{\mp}\phi_0\right) - \frac{c_4}{\sqrt{5}}\Theta\phi_{\mp1}^*, \tag{3c}$$

where $L = -\hbar^2/2m\nabla^2 + V_T(\mathbf{r}) + c_0(|\phi_2|^2 + |\phi_1|^2 + |\phi_0|^2 + |\phi_{-1}|^2 + |\phi_{-2}|^2)$.

In the dimensionless form our coupled field equations become

$$i\frac{\partial\phi_2}{\partial t} = L\phi_2 + \tau_2(2f^z\phi_2 + f^-\phi_1) + \frac{\tau_4}{\sqrt{5}}\Theta\phi_{-2}^*, \tag{4a}$$

$$i\frac{\partial\phi_1}{\partial t} = L\phi_1 + \tau_2\left(f^+\phi_2 + f^z\phi_1 + \frac{\sqrt{6}}{2}f^-\phi_0\right) - \frac{\tau_4}{\sqrt{5}}\Theta\phi_{-1}^*, \tag{4b}$$

$$i\frac{\partial\phi_0}{\partial t} = L\phi_0 + \tau_2\frac{\sqrt{6}}{2}(f^+\phi_1 + f^-\phi_{-1}) + \frac{\tau_4}{\sqrt{5}}\Theta\phi_0^*, \tag{4c}$$

$$i\frac{\partial\phi_{-1}}{\partial t} = L\phi_{-1} + \tau_2\left(f^-\phi_{-2} - f^z\phi_{-1} + \frac{\sqrt{6}}{2}f^+\phi_0\right) - \frac{\tau_4}{\sqrt{5}}\Theta\phi_1^*, \tag{4d}$$

$$i\frac{\partial\phi_{-2}}{\partial t} = L\phi_{-2} + \tau_2(-2f^z\phi_{-2} + f^+\phi_{-1}) + \frac{\tau_4}{\sqrt{5}}\Theta\phi_2^*, \tag{4e}$$

where $L = -\nabla^2 + V_T(\mathbf{r}) + \tau_0(|\phi_2|^2 + |\phi_1|^2 + |\phi_0|^2 + |\phi_{-1}|^2 + |\phi_{-2}|^2)$. Here wave functions, time, and spatial coordinates are measured in the units of $\frac{1}{(\hbar/2mw_z)^{3/4}}$, $w_z^{-1}$, and $(\hbar/2mw_z)^{1/2}$, respectively. Also here $\tau_0 = \frac{8\pi(4a_2+3a_4)}{7b_0}$, $\tau_2 = \frac{8\pi(a_4-a_2)}{7b_0}$, $\tau_4 = \frac{8\pi(7a_0-10a_2+3a_4)}{7b_0}$, and $b_0 = \sqrt{\frac{\hbar}{2mw_z}}$.

### A. Modulation instability analysis

The non-spin-mixing or the spin-polarized state of the system represented by stable *stationary* solutions have a constant population of each component and the wave functions for all spin components maintain the same spatial profile during the time evolution resulting from single-mode approximation (SMA). However, the above coupled equations give the spin-mixing dynamics [5,10,21] during the time evolution of the condensate (also shown in figures). For finding the stable *stationary* solution of the system we used the following ansatz:

$$\phi_j(\mathbf{r},t) = \sqrt{n_j(\mathbf{r})}e^{-i\mu_j t + i\theta_j}, \tag{5}$$

where $j = 2,1,0,-1,-2$ and $\theta_j$'s are relative phases of each component with respect to $\phi_0$, where $(\theta_0 = 0)$ and $\mu_j$ are the respective chemical potentials. Also, $n_2 + n_1 + n_0 + n_{-1} + n_{-2} = n$ is the total density of spinor condensate.

By the substitution of the ansatz (5) into the dimensionless coupled field equations it is clear that the system will give stationary solutions only if $\mu_j = \mu$ and for particular values of $\theta_j$, hereafter called *phase-locked*. The same effective potential created by both the optical trap and the nonlinear interaction have spinor eigenfunctions $\sqrt{n_j(\mathbf{r})}$ as eigenmodes with same eigenvalue, $\mu$. Since eigenfunctions are proportional to each other, we represent $n_j$ as $n_j(\mathbf{r}) = r_j n(\mathbf{r})$. Here $r_j$ represents the population of each spinor component in time-independent state, with $r_2 + r_1 + r_0 + r_{-1} + r_{-2} = 1$. So five spinor components obey the same time-independent equation for the particular values of $r_j$ and $\theta_j$. That is,

$$[-\nabla^2 - \mu + V_T(\mathbf{r})]\sqrt{n(\mathbf{r})} + \kappa n(\mathbf{r})\sqrt{n(\mathbf{r})}. \tag{6}$$

Since only particular values of $\theta_j$'s are giving the stationary solutions, we look for such solutions. There exist two different *phase-locked* steady-state solutions for dimensionless coupled field equations depending on relative phases, populations in each spin component, and different values of the $\kappa$. The cases are as follows.

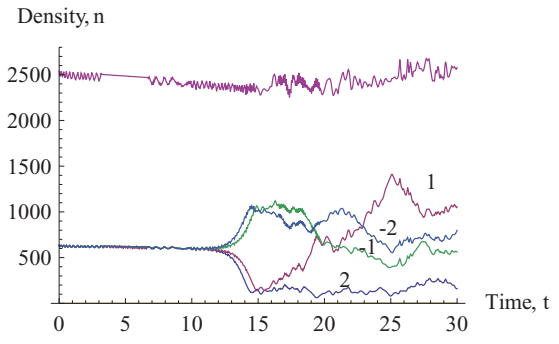


FIG. 1. (Color online) Time evolution of the central density, $n$ at $z = 0$ for the spinor components $\phi_{-2}(z)$, $\phi_{-1}(z)$, $\phi_1(z)$, $\phi_2(z)$ corresponding to the case 1. Parameters are $\tau_0 = 0.0889$, $\tau_2 = -0.000\,156$, $\tau_4 = 0.000\,623$, and chemical potential $\mu \approx 225$. The upper straight line showing the total density. In the figure 2, 1, $-1$, $-2$ stand for $\phi_2(z)$, $\phi_1(z)$, $\phi_{-1}(z)$, $\phi_{-2}(z)$ components, respectively.

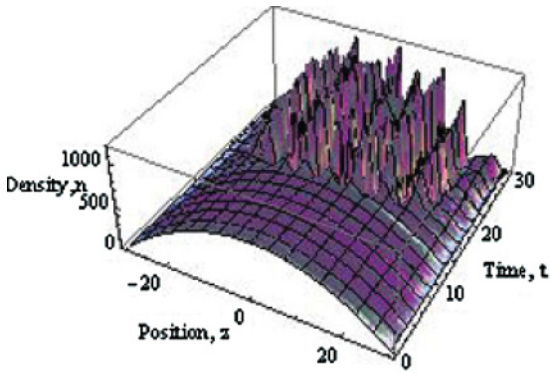


FIG. 2. (Color online) Time evolution of the 1D $\phi_{-1}(z)$ component for the case 1, showing the spatial development of the MI. The components $\phi_1(z)$, $\phi_2(z)$, $\phi_{-2}(z)$ behave similarly. Parameters are as in Fig. 1.

Case 1: $e^{i\theta_2} = e^{i\theta_1} = e^{i\theta_{-1}} = e^{i\theta_{-2}} = 1$, $\kappa = \tau_0 + \tau_2$, and populations are $r_2 = r_1 = r_{-1} = r_{-2} = \frac{1}{4}$ and $r_0 = 0$.

Case 2: $e^{i\theta_2} = e^{i\theta_{-2}} = 1$, $e^{i\theta_1} = e^{i\theta_{-1}} = i$, $\kappa = \tau_0 + \frac{\tau_4}{5}$, and populations are $r_2 = r_1 = r_0 = r_{-1} = r_{-2} = \frac{1}{5}$.

These two solutions represent the general stationary solutions of Eq. (4), which give spin-polarized states. In the spin-polarized states each component has a constant population. When we compared these stationary solutions to the ground-state phases of $F = 2$ spinor condensate [16] for the magnetic field free case, it is observed that our solutions are not a ground state for any phase. So our stationary solutions represent actually the equilibrium stationary states. With the stationary solutions, we are doing the instability analysis of spin polarized states. The above solutions resulting from the transformation of five-component equations to a single stationary equation. Hence, there are two cases. Here the time-independent mean field spin is $f = |f^x|$ with $f^y = f^z = 0$. One can apply the condition of phases (ferromagnetic, polar, or cyclic) to the stationary solutions. In each phase, the coupling constants are different [34] for magnetic field free case and hence the constant $\kappa$ varying with change in coupling constants. The ground-state energies of three phases are $\epsilon^F = 4\tau_2$, $\epsilon^{AF} = \tau_4/5$, and $\epsilon^C = 0$. As a result of different $\kappa$, we are getting six stationary solutions. However, it is possible to show that results arising from the manipulation of these six solutions are same as that of the results obtained by applying

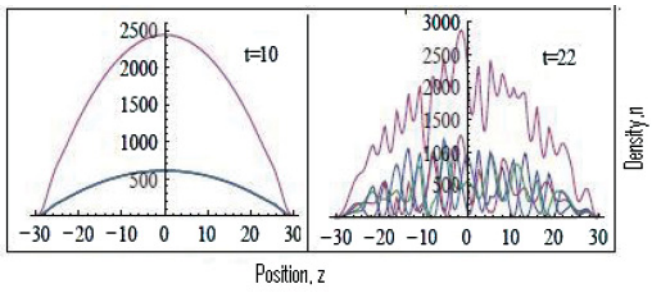


FIG. 3. (Color online) Spatial intensity profiles of the original spinor components, $\phi_j (j = 2,1,-1,-2)$, showing spin domain fragmentation (forming localized condensate domains). Parameters are as in Fig. 1.

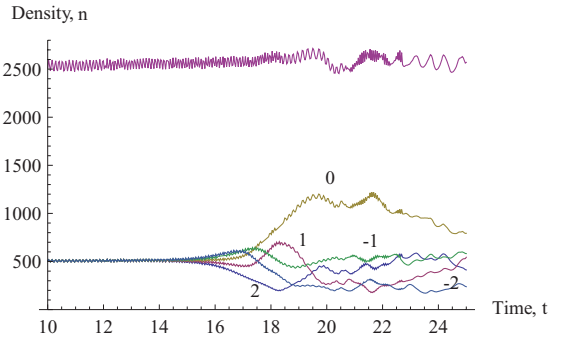


FIG. 4. (Color online) Time evolution of the central density $n(0)$ for the spinor components $\phi_{-2}(z)$, $\phi_{-1}(z)$, $\phi_1(z)$, $\phi_2(z)$, $\phi_0(z)$ corresponding to the case 2. Parameters are as in Fig. 1. The upper straight line showing the total density.

the conditions of three phases (conditions are given below) to the eigenvalues resulting from the general stationary solutions or matrix A (described below). It means that the conditions of phases given before or after the manipulation of the matrix A are equal. So for our further analysis we follow the latter method.

For the MI analysis, the exponential growth of the stationary homogenous condensate [24–31], we are adding a small perturbation to the homogenous solutions $\phi_j$ of the form

$$\phi_j(\mathbf{r},t) = [\sqrt{n_j(\mathbf{r})} + \delta\phi_j]e^{i\theta_j - i\mu t}. \tag{7}$$

It is clear that if any of the condensate phases show MI then we can observe the exponential growth of the stationary homogenous condensate in that particular phase and constant density solutions corresponding to the stationary phase relations in the cases 1 and 2 have the form $n_j^h = \frac{\mu}{\kappa}$. Then ansatz (7) becomes

$$\phi_j = \left(\sqrt{n_j^h} + \delta\phi_j\right)e^{-i\mu t + i\theta_j}. \tag{8}$$

We substitute (8) into the dimensionless coupled field equations to get the equations for $\delta\phi_j$; meanwhile, we linearize around the homogenous solutions and omit the terms containing $V_T$. After taking the perturbation of the form $\delta\phi_j = (u_j + iv_j)\cos(\mathbf{kr})e^{wt}$ [where $\mathbf{k} = (k_x,k_y,k_z)$] and using cases 1 and 2 we go for MI analysis using the equations for

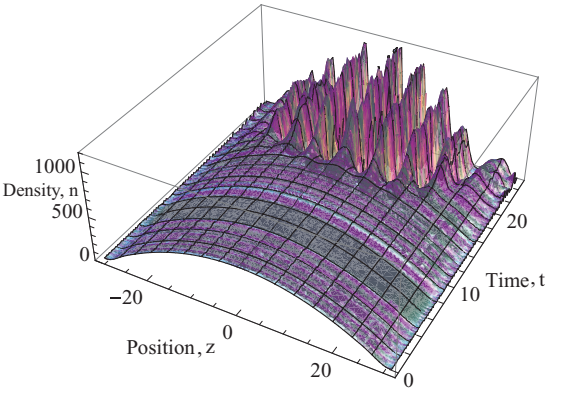


FIG. 5. (Color online) Time evolution of the $\phi_2(z)$ component for case 2, showing the spatial development of the MI. The components $\phi_1(z)$, $\phi_{-1}(z)$, $\phi_{-2}(z)$, and $\phi_0(z)$ behave similarly. Parameters are as in Fig. 1.

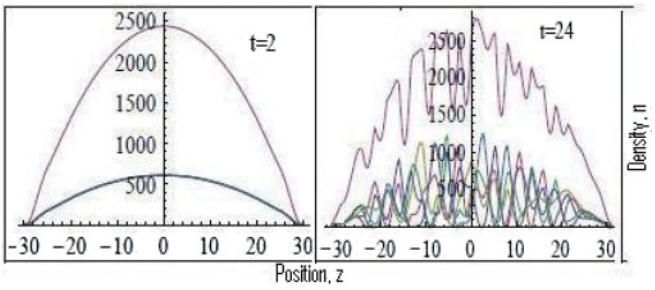


FIG. 6. (Color online) Spatial intensity profiles of the original spinor components, $\phi_j (j = 2,1,0,-1,-2)$, showing spin domain fragmentation. Parameters are as in Fig. 1 (for case 2).

$\delta\phi_j$. From our form of perturbation, it is clear that for the real values of the $w$ spinor condensate will show the MI.

On the substitution of $\delta\phi_j = (u_j + iv_j)\cos(\mathbf{kr})e^{wt}$ in the equations for $\delta\phi_j$ these equations will become $\hat{A}\Omega^T = 0$, where $\Omega = (u_j, v_j)$, with $j = 2,1,0,-1,-2$. Then we solve $\det(\hat{A}) = 0$ with respect to $w$ (perturbation frequency). Because of the complexity of solving this big matrix we take that two of the components are equal and all others equal to zero for the simplification. Then the eigenvalues are as follows.

For case 1,

$$w_1^2 = \frac{1}{25(\tau_0+\tau_2)^2}\big\{-25(2\mu\mathbf{k}^2+\mathbf{k}^4)\tau_0^2 - 25(\mu-\mathbf{k}^2)^2\tau_2^2 + 20\mu(\mu-\mathbf{k}^2)\tau_2\tau_4 - 3\mu^2\tau_4^2 + 10\tau_0 \times [5(\mu^2-\mathbf{k}^4)\tau_2 - \mu(\mu+2\mathbf{k}^2)\tau_4]\big\}, \tag{9a}$$

$$w_2^2 = \frac{1}{25(\tau_0+\tau_2)^2}\big[-25\mathbf{k}^4\tau_0^2 + 50\mathbf{k}^2(\mu-\mathbf{k}^2)\tau_0\tau_2 - 25(\mu-\mathbf{k}^2)^2\tau_2^2 + \mu^2\tau_4^2\big], \tag{9b}$$

$$w_3^2 = \frac{-1}{25(\tau_0+\tau_2)^2}[5\mathbf{k}^4\tau_0 + 5(7\mu+\mathbf{k}^2)\tau_2 - \mu\tau_4) \times (5\mathbf{k}^2\tau_0 - 5(\mu-\mathbf{k}^2)\tau_2 + \mu\tau_4], \tag{9c}$$

$$w_4^2 = \frac{-1}{25(\tau_0+\tau_2)^2}[5\mathbf{k}^4\tau_0 + 5(\mu+\mathbf{k}^2)\tau_2 - \mu\tau_4] \times [5\mathbf{k}^2\tau_0 - 5(\mu-\mathbf{k}^2)\tau_2 + \mu\tau_4]. \tag{9d}$$

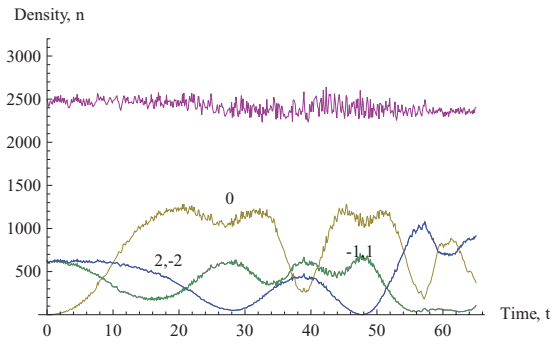


FIG. 7. (Color online) Time evolution of the central density $n(0)$ for the spinor components $\phi_{-2}(z)$, $\phi_{-1}(z)$, $\phi_1(z)$, $\phi_2(z)$, $\phi_0(z)$ corresponding to case 1. Parameters are $\tau_0 = 0.1085$, $\tau_2 = 0.001\,792$, $\tau_4 = -0.000\,187$, and chemical potential $\mu \approx 275$.

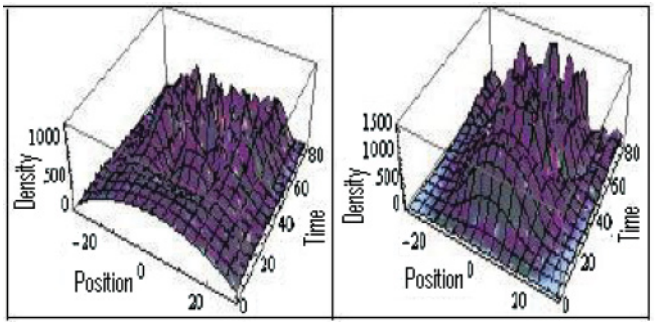


FIG. 8. (Color online) Time evolution of the $\phi_2(z)$ and $\phi_0(z)$ component for case 1, showing the spatial development of the MI. The components $\phi_1(z)$, $\phi_{-1}(z)$, and $\phi_{-2}(z)$ behave similarly to $\phi_2(z)$. Parameters are as in Fig. 7.

For case 2,

$$w_1^2 = -5(2\mu\mathbf{k}^2 + \mathbf{k}^4), \tag{10a}$$

$$w_2^2 = \frac{-1}{(5\tau_0+\tau_4)}\{5[5\mathbf{k}^4\tau_0 + \mathbf{k}^2(-2\mu+\mathbf{k}^2)\tau_4]\}, \tag{10b}$$

$$w_3^2 = \frac{-1}{(5\tau_0+\tau_4)}\{5\mathbf{k}^2[5\mathbf{k}^2\tau_0 + 40\mu\tau_2 + (-2\mu+\mathbf{k}^2)\tau_4]\}, \tag{10c}$$

$$w_4^2 = \frac{-1}{(5\tau_0+\tau_4)}\{5\mathbf{k}^2[5\mathbf{k}^2\tau_0 + 10\mu\tau_2 + (-2\mu+\mathbf{k}^2)\tau_4]\}. \tag{10d}$$

From recent studies [34] it is clear that for the ferromagnetic phase $\tau_2 < 0$ and $\tau_4 > 0$, for the antiferromagnetic (polar) phase $\tau_2 > 0$ and $\tau_4 < 0$, and for the cyclic phase $\tau_2 > 0$ and $\tau_4 > 0$. When applying these conditions we will get some real eigenvalues $w_i (i = 1,2,3,4)$ in all cases except case 2 of polar state for some real positive values of $\mathbf{k}$ because of small values of $\mathbf{k}$ and larger values of the chemical potential.

For example, we take $w_3$ from case 1. So it is clear that $[5\mathbf{k}^4\tau_0 + 5(7\mu+\mathbf{k}^2)\tau_2 - \mu\tau_4][5\mathbf{k}^2\tau_0 - 5(\mu-\mathbf{k}^2)\tau_2 + \mu\tau_4]$ should be negative to show modulation instability.

For the ferromagnetic case $\tau_2 < 0$ and $\tau_4 > 0$. So we will get a negative value for $[5\mathbf{k}^4\tau_0 + 5(7\mu+\mathbf{k}^2)\tau_2 - \mu\tau_4]$ and a positive one for $[5\mathbf{k}^2\tau_0 - 5(\mu-\mathbf{k}^2)\tau_2 + \mu\tau_4]$. As a result, $w_3$ becomes positive.

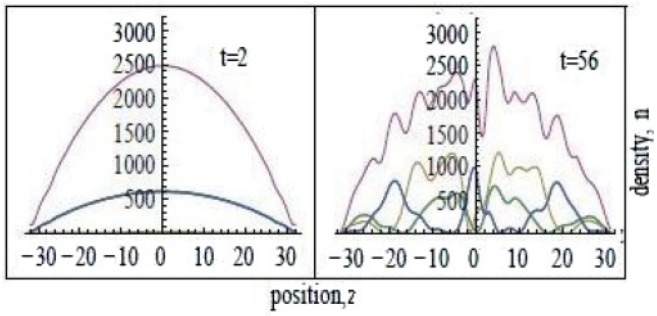


FIG. 9. (Color online) Spatial intensity profiles of the original spinor components, $\phi_j (j = 2,1,0,-1,-2)$, showing spin domain fragmentation. Parameters are as in Fig. 7 (for case 1).

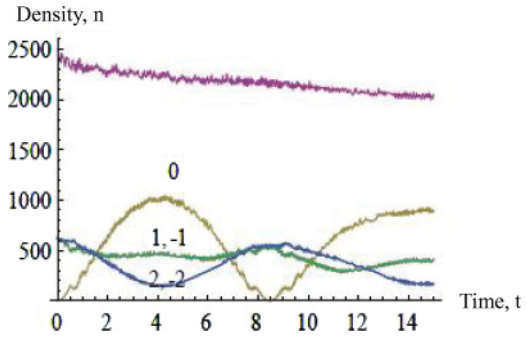


FIG. 10. (Color online) Time evolution of the central density $n(0)$ for the spinor components $\phi_{-2}(z)$, $\phi_{-1}(z)$, $\phi_1(z)$, $\phi_2(z)$, and $\phi_0(z)$ corresponding to case 1. Parameters are $\tau_0 = -0.6764$, $\tau_2 = 0.0164$, $\tau_4 = 0.0382$, and chemical potential $\mu \approx 1650$.

For the polar phase we will get positive values for $[5\mathbf{k}^4\tau_0 + 5(7\mu + \mathbf{k}^2)\tau_2 - \mu\tau_4]$ and negative ones for $[5\mathbf{k}^2\tau_0 - 5(\mu - \mathbf{k}^2)\tau_2 + \mu\tau_4]$ because $\tau_2 > 0$ and $\tau_4 < 0$. So effectively $w_3$ is positive.

For the cyclic case it is clear that $[5(7\mu + \mathbf{k}^2)\tau_2 - \mu\tau_4]$ is positive and $[-5(\mu - \mathbf{k}^2)\tau_2 + \mu\tau_4]$ is negative ($\tau_2 > 0$ and $\tau_4 > 0$). So we get positive values for $w_3$.

Also, it is clear that in case 2 all eigenvalues are imaginary when $\tau_2 > 0$ and $\tau_4 < 0$ (polar phase). So from case 1 and case 2 it is clear that at least one of the eigenvalues is real for the polar, ferro, and cyclic cases except for case 2 of the polar phase. So except for case 2 of the polar phase all other cases show *modulation instability*.

Since we have made an approximation like some populations are zero, we have to prove it numerically. Also, it is possible to prove the same result without these approximations analytically.

## III. NUMERICAL ANALYSIS

From recent studies it was clear that, if the characteristic spatial extent of the condensate, $l$ (in dimensionless units), is larger than the largest length scale of the spatial patterns due to the MI, $L = k_{\min}^{-1}$, the instability of the homogeneous condensate is bound to trigger the formation of the complex patterns in the trapped condensate [14]. Whenever this condition is satisfied by the spinor condensate we can go for MI analysis of the trapped condensate. The value of $k_{\min}$ can be calculated from one of the eigenvalues by minimizing it.

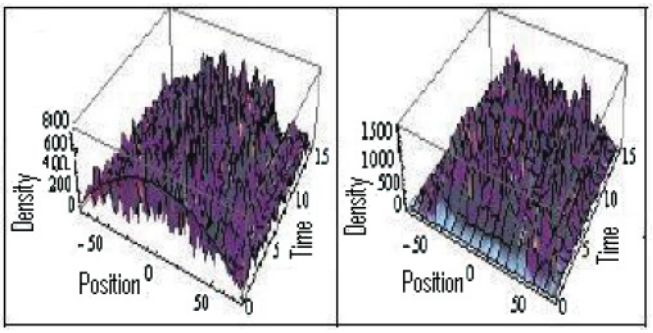


FIG. 11. (Color online) Time evolution of the $\phi_1(z)$ and $\phi_0(z)$ components for case 1, respectively, showing the spatial development of the MI. The components, $\phi_{-1}(z)$, $\phi_2(z)$, and $\phi_{-2}(z)$ behave almost similarly to $\phi_1(z)$. Parameters are as in Fig. 10.

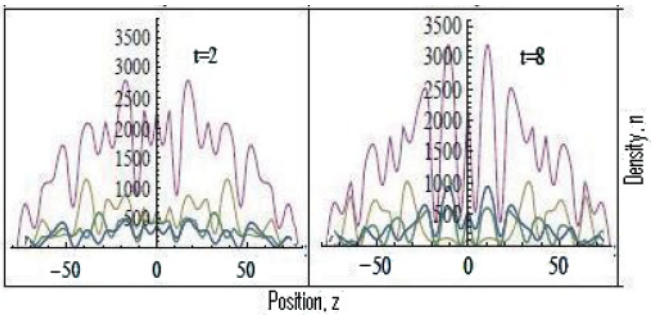


FIG. 12. (Color online) Spatial intensity profiles of the original spinor components, $\phi_j (j = 2,1,0,-1,-2)$, showing spin domain fragmentation. Parameters are as in Fig. 10.

For MI analysis we first assume that our trapping potential is a cigar-shaped harmonic potential of the form $V_T(x,y,z) = \frac{m}{2}(w_x^2x^2 + w_y^2y^2 + w_z^2z^2)$ [32]. From the dimensionless coupled equation it is clear that this potential will have the form $V_T(x,y,z) = \frac{1}{4}[(\frac{w_x}{w_z})^2x^2 + (\frac{w_y}{w_z})^2y^2 + z^2]$, where $w_x$, $w_y$, and $w_z$ are the trap frequencies in the $x$ direction, $y$ direction, and $z$ direction, respectively. If we are approximating confinement in the $x$ and $y$ directions (transverse) to be larger than in the $z$ direction and the transverse wave function to be the ground-state wave function of harmonic oscillator then the wave function associated with the spin state $j$ can be written as $\phi_j(\mathbf{r},t) = \phi_h(x,y)\phi_j(z,t)$, where $z$ is the direction of weak confinement and $\phi_h(x,y)$ is the ground-state wave function of the two-dimensional harmonic oscillator. So in our coupled equation, $L$ becomes $L = -\frac{\partial^2}{\partial z^2} + \frac{1}{4}z^2 + \tau_0(|\phi_2|^2 + |\phi_1|^2 + |\phi_0|^2 + |\phi_{-1}|^2 + |\phi_{-2}|^2)$.

Using case 1 and case 2 of the stationary phase-locked solutions we solved the 1D equivalent of coupled partial differential equations numerically by taking the initial condition $\phi_j(z) = \sqrt{r_j n(z)}e^{i\theta_j}$ as for the $F = 1$ case, where $n(z)$ is the 1D spatial profile determined from Eq. (6). We calculate the numerical values of the $\tau_0$, $\tau_2$, $\tau_4$ from the experimentally obtained scattering lengths [20].

The results of numerical calculation for ferromagnetic case 1 are shown in Figs. 1, 2, and 3 and for ferromagnetic case 2 are shown in Figs. 4, 5, and 6.

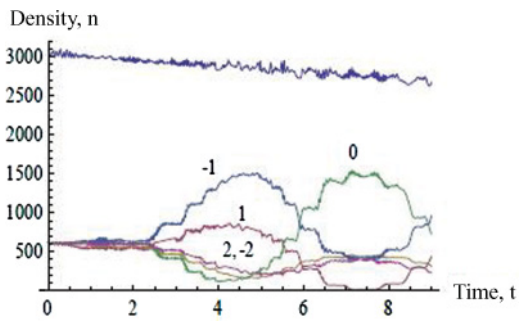


FIG. 13. (Color online) Time evolution of the central density $n(0)$ for the spinor components $\phi_{-2}(z)$, $\phi_{-1}(z)$, $\phi_1(z)$, $\phi_2(z)$, and $\phi_0(z)$ corresponding to case 2. Parameters are $\tau_0 = -0.6764$, $\tau_2 = 0.0164$, $\tau_4 = 0.0382$, and chemical potential $\mu \approx 1650$.

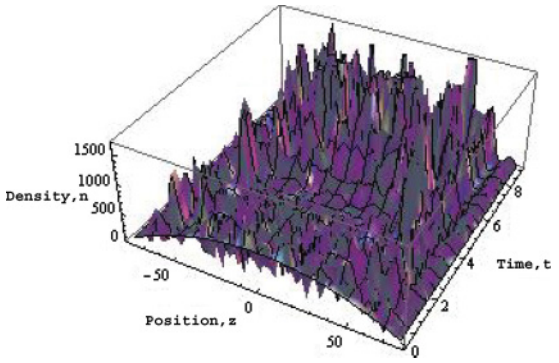


FIG. 14. (Color online) Time evolution of the $\phi_0(z)$ component for case 2, showing the spatial development of the MI. Other components behave similarly. Parameters are as in Fig. 13.

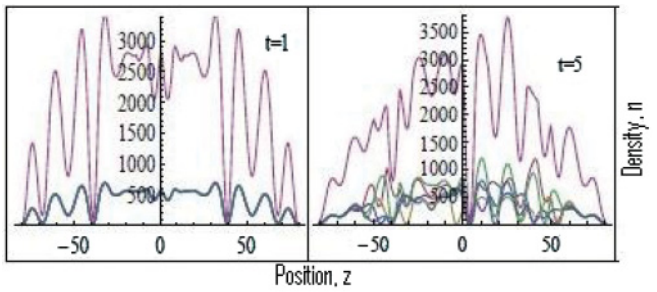


FIG. 15. (Color online) Spatial intensity profiles of the original spinor components, $\phi_j (j = 2,1,0,-1,-2)$, showing spin domain fragmentation. Parameters are as in Fig. 13.

For the ferromagnetic case 1, results show that instability first destroys the non-spin-mixing stationary state leading to population transfer between components (Fig. 1). Although we have started with four components that are equal and the zeroth component is zero, after some time we observed that the $\phi_1$, $\phi_{-1}$, and $\phi_{-2}$ components contribute the major portion of the condensate. There is no evolution of the $\phi_0$ component. This shows the spin mixing in the ferromagnetic phase. Figure 2 shows the periodic modulation of the condensates due to the modulation instability of the trapped condensates and Fig. 3 shows the spatial fragmentation (spin domain fragmentation). Also it is clear that the total density is also fluctuating by conserving the particle numbers.

When compared with case 1, in case 2 we observed the evolution of the $\phi_0$ component. After some time even all components presented initially, the $\phi_0$ component contributing the major portion of the spinor condensate (Fig. 4) as a result of spin mixing. Figures 5 and 6 show the periodic spatial modulation and fragmentation of the components, respectively.

In case 1 of the polar state dynamical instability causes the evolution of the initially absent component at a later time. That is, even the $\phi_0$ component was taken as zero initially; we observe the evolution of this component as time passes. Also, evolution of $\phi_2$ and $\phi_{-2}$ (same for $\phi_1$ and $\phi_{-1}$) are same (Fig. 7) or no spatial separation between the $m = \pm 2$ state. It is the necessary condition for BEC to be antiferromagnetic. Also, this figure shows the stability of $m_F = \pm 2$ components. This result is almost similar to the result in [21]. Figure 8 shows that periodic modulations of all components are not similar and Fig. 9 shows spatial fragmentation is not denser when compared with ferromagnetic cases.

Spin mixing and periodic modulation happen earlier for cyclic cases. As in the polar phase here also we can see the evolution of the $\phi_0$ component due to the instability (initially it is absent). In case 1, the density of the $\phi_1$ and $\phi_{-1}$ components are almost constant during the evolution of the spinor condensate (Fig. 10). Figures 11 and 12 show periodic modulation, not similar for all components, and spatial fragmentation, respectively.

For case 2, with increasing time density of $\phi_1$ and $\phi_{-1}$ components show fluctuations. However, the fluctuation in density during the evolution of these components is almost constant in case 1. Here the periodic modulations of all the components are almost similar (see Figs. 13, 14, and 15).

From the figures of the evolution of the central density for the spinor components it is clear that dynamics of $F = 2$ spinor condensate also obey the total spin conservation.

## IV. CONCLUSION

We have shown the possibility of modulation instability in all phases of $F = 2$ spinor condensate analytically and numerically from the multicomponent GP equations that describe evolution of the order parameters. This result is different from MI of the $F = 1$ spinor case, where the polar phase is free from the modulation instability phenomena. In the polar phase both analyses have shown that linear instability depends upon the cases resulting from steady-state solutions. This gives the information that modulation instability depends on the relative phase between the components and initial population for the polar phase. Observations of the spin-mixing dynamics by numerical analysis show the resemblance with earlier studies and results like dissimilarity in periodic modulations of components and spin domain fragmentation give the scope of future works.

## ACKNOWLEDGMENTS

K.P. thanks DST, DAE-BRNS, and UGC, Government of India, for the financial support through research projects. The authors are grateful to Dr. Amitava Choudhuri for fruitful discussions and also would like to thank the referee for valuable comments.

[1] M. H. Anderson, J. R. Ensher, M. R. Mathews, C. E. Wieman, and E. A. Cornell, Science **269**, 198 (1995).

[2] K. B. Davis, M.-O. Mewes, M. R. Andrews, N. J. van Druten, D. S. Durfee, D. M. Kurn, and W. Ketterle, Phys. Rev. Lett. **75**, 3969 (1995).

[3] C. C. Bradley, C. A. Sackett, J. J. Tollett, and R. G. Hulet, Phys. Rev. Lett. **75**, 1687 (1995).

[4] M.-S. Chang, C. D. Hamley, M. D. Barrett, J. A. Sauer, K. M. Fortier, W. Zhang, L. You, and M. S. Chapman, Phys. Rev. Lett. **92**, 140403 (2004).

[5] H. Schmaljohann, M. Erhard, J. Kronjager, M. Kottke, S. van Staa, L. Cacciapuoti, J. J. Arlt, K. Bongs, and K. Sengstock, Phys. Rev. Lett. **92**, 040402 (2004).
[6] W. Zhang, D. L. Zhou, M. S. Chang, M. S. Chapman, and L. You, Phys. Rev. A **72**, 013602 (2005).
[7] C. K. Law, H. Pu, and N. P. Bigelow, Phys. Rev. Lett. **81**, 5257 (1998).
[8] M.-S. Chang, Q. Qin, W. Zhang, Li You, and M. S. Chapman, Nat. Phys. **1**, 111 (2005).
[9] T. Isoshima, K. Machida, and T. Ohmi, Phys. Rev. A **60**, 4857 (1999).
[10] H. Pu, C. K. Law, S. Raghavan, J. H. Eberly, and N. P. Bigelow, Phys. Rev. A **60**, 1463 (1999).
[11] T. L. Ho, Phys. Rev. Lett. **81**, 742 (1998).
[12] T. Ohmi and K. Machida, J. Phys. Soc. Jpn. **67**, 1822 (1998).
[13] J. Stenger, S. Inouye, D. M. Stamper-Kurn, H.-J. Miesner, A. P. Chikkatur, and W. Ketterle, Nature (London) **396**, 345 (1998).
[14] N. P. Robins, W. Zhang, E. A. Ostrovskaya, and Y. S. Kivshar, Phys. Rev. A **64**, 021601 (2001).
[15] L. Li, Z. Li, B. A. Malomed, D. Mihalache, and W. M. Liu, Phys. Rev. A **72**, 033611 (2005).
[16] J.-P. Martikainen and K.-A. Suominen, J. Phys. B **34**, 4091 (2001).
[17] M. Takahashi, T. Mizushima, and K. Machida, J. Low Temp. Phys. **158**, 58 (2010).
[18] V. A. Brazhnyi and V. V. Konotop, Mod. Phys. Lett. B **18**, 627 (2004).
[19] J. S. Huang, Z. W. Xie, M. Zhang, and L. F. Wei, J. Phys. B **43**, 065305 (2010).
[20] C. V. Ciobanu, S. K. Yip, and T-L. Ho, Phys. Rev. A **61**, 033607 (2000).
[21] H. Saito and M. Ueda, Phys. Rev. A **72**, 053628 (2005).
[22] E. V. Goldstein and P. Meystre, Phys. Rev. A **55**, 2935 (1997).
[23] M. Uchiyama, J. Ieda, and M. Wadati, J. Phys. Soc. Jpn. **76**, 074005 (2007).
[24] G. P. Agrawal, Phys. Rev. Lett. **59**, 880 (1987).
[25] T. S. Raju, P. K. Panigrahi, and K. Porsezian, Phys. Rev. A **71**, 035601 (2005).
[26] R. Murali and K. Porsezian, Physica D **239**, 1 (2010).
[27] J.-S. Huang, Z.-W. Xie, M. Zhang, and L.-F. Wei1, J. Phys. B **43**, 065305 (2010).
[28] K. Kasamatsu and M. Tsubota, Phys. Rev. A **74**, 013617 (2006).
[29] K. Kasamatsu and M. Tsubota, Phys. Rev. Lett. **93**, 100402 (2004).
[30] L. Wu, J-F. Zhang, and L. Li, New J. Phys. **9**, 69 (2007).
[31] L. Sheng-Chang and D. Wen-Shan, Chin. Phys. B **18**, 4177 (2009).
[32] H. Wang, J. Comput. Phys. **230**, 6155 (2011).
[33] A. M. Turner, R. Barnett, E. Demler, and A. Vishwanath, Phys. Rev. Lett. **98**, 190404 (2007).
[34] M. Ueda and M. Koashi, Phys. Rev. A **65**, 063602 (2002).